

PolInSAR Coherence Region Modeling and Inversion: The Best Normal Matrix Approximation Solution

Yi Cui, *Member, IEEE*, Yoshio Yamaguchi, *Fellow, IEEE*, Hiroyoshi Yamada, *Senior Member, IEEE*, and Sang-Eun Park, *Member, IEEE*,

Abstract—In this paper, we address the theoretical aspects of coherence region modeling and its inversion methods for polarimetric interferometric SAR (PolInSAR). Instead of only considering the geometrical shape of the coherence region, we focus on directly modeling the whitened interferometric cross-correlation matrix of the PolInSAR data. In particular, we consider three classes of generic scattering models that respectively contain single, double and triple phase centers within one resolution cell. We then demonstrate, for each class, that the modeled whitened interferometric cross-correlation matrix is normal. Based on this property, we propose, for each case, efficient algorithms to obtain the best normal matrix approximation solution for model inversion from the observed whitened interferometric cross-correlation matrix. In addition, we show how a simple and effective criterion can be designed from the derived solutions for model validation. Finally, we verify the solutions with both simulated and real data. The results prove the proposed method to be a very promising tool for PolInSAR applications.

Index Terms—Polarimetric interferometric SAR (PolInSAR), coherence region modeling, model inversion, whitened interferometric cross-correlation matrix, best normal matrix approximation.

I. INTRODUCTION

IN past decades, polarization diversity has been extensively exploited to understand the scattering mechanisms in synthetic aperture radar (SAR) images [1]–[7]. Due to the sensitivity of the wave polarization states to the physical and geometrical structure of the targets, the potential capability of polarimetric SAR (PolSAR) to discriminate multiple scatterers beyond imaging resolutions has been demonstrated by eigen-based [8] or model-based decomposition [9]. However, since such discrimination is only based on the polarization-dependent backscatter responses, the spatial position of different scatterers cannot be inferred from a single PolSAR dataset. Interferometric SAR (InSAR), on the other hand, enables 3-dimensional imaging to render the earth topography by dual acquisitions [10]. Nevertheless, single-baseline interferometry cannot provide fully tomographic information [11]. Strictly speaking, it is only able to determine one phase center on the ground whereas in the presence of multiple scatterers

of different height distribution, conventional InSAR fails in discrimination.

Polarimetric interferometric SAR (PolInSAR) combines both advantages of radar polarimetry and interferometry. The key concept of PolInSAR was first introduced by Cloude and Papathanassiou in [12] where they showed that polarization plays a significant role in the variation of the interferometric coherence. They further demonstrated that the optimal coherence values can be successfully used for tree height inversion [13]. Later, it was pointed by Flynn and Tab [14], [15] and Colin et al. [16] that the behavior of the PolInSAR coherence, i.e., the coherence region, is equivalent to the numerical range of the whitened interferometric cross-correlation matrix (see Section II-B for definition). Based on this formulation, Colin et al. [16] devised an alternative coherence optimization algorithm which proves useful for phase estimation of point scatterers.

Meanwhile, several scattering models have been also proposed for analysis of PolInSAR data. Among them, the random volume over ground (RVoG) [13], [17] is probably the most recognized one that encodes double phase centers. It has been shown that the coherence region of the RVoG model is a line segment of which the slope as well as the end points contains the essential information [18]. Therefore, the task of model inversion becomes estimation of the line parameters from the measured coherence region. Cloude et al. [18] did this by least squares fitting the coherence values of typical scattering mechanisms. Ferro-Famil et al. [19] addressed the problem by a maximum likelihood approach. More recently, Lopez-Martinez et al. [20] proposed the affine transformation method to estimate the line segment. Another widely used PolInSAR model has been the summation of single scatterers which was first considered by Yamada et al. [21] for forest height inversion. They showed that parameter estimation of the model is virtually equivalent to array signal processing and can be solved by the ESPRIT algorithm. Guillaso et al. [22], [23] further applied the ESPRIT algorithm for urban characterization, whose works are the first ones to evaluate such method for the separation of isolated scattering phase centers in the context of building layovers. Similar problem was also addressed by Colin et al. in [16] where the coherence of each single scatterer is related to the boundary point of the coherence region.

We have seen that inversion of the model parameters is often accomplished by examining the geometrical shapes of the

Y. Cui, Y. Yamaguchi, H. Yamada are with the Department of Information Engineering, Niigata University, Ikarashi 8050-2, Nishi-ku, Niigata, 950-2181, Japan (e-mail: cuiyi.trea@gmail.com; yamaguch@ie.niigata-u.ac.jp; yamada@ie.niigata-u.ac.jp). S.-E. Park is with the Geoinformation Engineering, Sejong University, 209 Neungdong-ro, Gwangjin-gu, Seoul 143-747, Korea (e-mail: separk@sejong.ac.jp)

coherence region for fitting of points or line segments. However, since the coherence region is equivalent to the numerical range which in turn is uniquely determined by the whitened interferometric cross-correlation matrix, model inversion can be essentially done in a more algebraic way by extraction of this matrix from the noisy observable. Note that this should be distinguished from the statistical mission of speckle reduction which aims to estimate the PolInSAR coherency matrix data [24] (see also Section II-A). Indeed, in the absence of thermal and temporal decorrelation and with sufficiently large multi-looking, the whitened interferometric cross-correlation matrix computed from the reconstructed PolInSAR coherency does asymptotically approach the true one. Unfortunately, very high number of looks is often practically unavailable due to, e.g., scene heterogeneity. Thus the task herein defined is better regarded as a refined step that follows speckle filtering, that is, to infer the whitened interferometric cross-correlation matrix that is consistent with the assume scattering model, from the filtered PolInSAR data.

In this paper, we will show that such a task can be accomplished by effectively exploiting the special structure of the whitened interferometric cross-correlation matrix. Especially, we will demonstrate that for a wide class of scattering models, the whitened interferometric cross-correlation matrix should be normal. The property consequently motivates us to derive very efficient algorithms to obtain the best normal matrix approximation solution for model inversion.

This paper is organized as follows. In Section II we give a brief review of PolInSAR. In Sections III, Section IV, and Section V we respectively discuss the scattering models consisting of single, double, and triple phase centers and we each derive the algorithms for the corresponding best normal matrix approximation solution. In Section VI, we show how to use the best normal matrix approximation solution to validate the scattering models. In Section VII, we demonstrate the effectiveness of the solution by simulation and in Section VIII we provide the experimental result on real PolInSAR dataset. Finally, Section IX is the conclusion.

II. POLARIMETRIC SAR INTERFEROMETRY

A. PolInSAR Data

A single-baseline PolInSAR system measures, by dual polarimetric acquisitions, two complex scattering matrices for each resolution cell. In the case of reciprocal propagation media, either scattering matrix can be equivalently represented by the corresponding Pauli-vector:

$$\mathbf{k} = \frac{1}{\sqrt{2}} \begin{bmatrix} S_{HH} + S_{VV} \\ S_{HH} - S_{VV} \\ 2S_{HV} \end{bmatrix}, \quad (1)$$

where S_{HH}, S_{HV}, S_{VV} are the backscattering coefficients in the horizontal/vertical polarization basis. Suppose \mathbf{k}_1 and \mathbf{k}_2 respectively denote the master and slave Pauli-vectors, then the concatenated vector can be formed by $[\mathbf{k}_1^T, \mathbf{k}_2^T]^T$ from which the polarimetric interferometric coherency matrix, \mathbf{T}_6 , is defined as:

$$\mathbf{T}_6 = \left\langle \begin{bmatrix} \mathbf{k}_1 \\ \mathbf{k}_2 \end{bmatrix} \begin{bmatrix} \mathbf{k}_1^H & \mathbf{k}_2^H \end{bmatrix} \right\rangle = \begin{bmatrix} \mathbf{T}_{11} & \mathbf{\Omega}_{12} \\ \mathbf{\Omega}_{12}^H & \mathbf{T}_{22} \end{bmatrix}, \quad (2)$$

where $\mathbf{T}_{ii} = \langle \mathbf{k}_i \mathbf{k}_i^H \rangle$ is the 3×3 polarimetric coherency matrix and $\mathbf{\Omega}_{12} = \langle \mathbf{k}_1 \mathbf{k}_2^H \rangle$ is the interferometric cross-correlation matrix. It is specially noted that the ensemble averaging operator $\langle \cdot \rangle$ should be differentiated from the ideal mathematical expectation. The former involves the finite multilooking effect such that both \mathbf{T}_{ii} and $\mathbf{\Omega}_{12}$ are subject to speckle to various degrees. This fact constitutes one major challenge when we are trying to infer exact scattering models from real PolInSAR data.

B. PolInSAR Coherence

The interferometric coherence for the PolInSAR data is given by [12]:

$$\gamma(\mathbf{w}_1, \mathbf{w}_2) = \frac{\mathbf{w}_1^H \mathbf{\Omega}_{12} \mathbf{w}_2}{\sqrt{\mathbf{w}_1^H \mathbf{T}_{11} \mathbf{w}_1} \sqrt{\mathbf{w}_2^H \mathbf{T}_{22} \mathbf{w}_2}}, \quad (3)$$

where \mathbf{w}_1 and \mathbf{w}_2 are two arbitrary 3×1 non-zero complex vectors of the same norms. In this paper we consider the single-mechanism variant of (3) under the constraint of $\mathbf{w}_1 = \mathbf{w}_2 = \mathbf{w}$, by the reasoning that $\mathbf{T}_{11} \approx \mathbf{T}_{22}$ with small spatial and temporal baseline. Consequently, (3) becomes:

$$\gamma(\mathbf{w}) = \frac{\mathbf{w}^H \mathbf{\Omega}_{12} \mathbf{w}}{\mathbf{w}^H \mathbf{T} \mathbf{w}}, \quad (4)$$

where $\mathbf{T} = (\mathbf{T}_{11} + \mathbf{T}_{22})/2$. By letting $\mathbf{v} = \mathbf{T}^{\frac{1}{2}} \mathbf{w}$, (4) can be further written as:

$$\gamma(\mathbf{v}) = \frac{\mathbf{v}^H \tilde{\mathbf{\Omega}}_{12} \mathbf{v}}{\mathbf{v}^H \mathbf{v}}, \quad (5)$$

where *the whitened interferometric cross-correlation matrix* is given by:

$$\tilde{\mathbf{\Omega}}_{12} = \mathbf{T}^{-\frac{1}{2}} \mathbf{\Omega}_{12} \mathbf{T}^{-\frac{1}{2}}. \quad (6)$$

Importantly, (5) allows to relate all the possible values of the interferometric coherence (i.e., the coherence region) with the concept of *numerical range* of $\tilde{\mathbf{\Omega}}_{12}$, which is defined as the set:

$$W(\tilde{\mathbf{\Omega}}_{12}) = \left\{ \frac{\mathbf{v}^H \tilde{\mathbf{\Omega}}_{12} \mathbf{v}}{\mathbf{v}^H \mathbf{v}} \mid \mathbf{v} \in \mathbb{C}^3, \mathbf{v} \neq \mathbf{0} \right\}. \quad (7)$$

Accordingly, the coherence region is mathematically equivalent to $W(\tilde{\mathbf{\Omega}}_{12})$ that solely depends on $\tilde{\mathbf{\Omega}}_{12}$. In general, determination of the numerical range of an arbitrary matrix has not been a trivial problem and intensive efforts have been devoted for its study [25], [26]. A comprehensive investigation of the numerical range in the context PolInSAR applications is also given by Neumann [27]. Interestingly, however, in certain special cases the numerical range can take a fairly regular form. In particular, the following theorem holds: [26]

Theorem 1. *Let \mathbf{A} be an $n \times n$ complex matrix. If \mathbf{A} is a normal matrix that is, if $\mathbf{A}\mathbf{A}^H = \mathbf{A}^H\mathbf{A}$, then $W(\mathbf{A})$ is the convex hull of the points in the complex plane corresponding to the eigenvalues of \mathbf{A} ; and the reverse is true for $n \leq 4$: if $W(\mathbf{A})$ is the convex hull of the eigenvalues of \mathbf{A} ($n \leq 4$), \mathbf{A} is normal.*

As a consequence, one may immediately see that if $\tilde{\mathbf{\Omega}}_{12}$ is normal, its coherence region will be a triangle whose vertices

correspond to the three eigenvalues of $\tilde{\Omega}_{12}$. Depending on the location of the eigenvalues the triangle can also degenerate into a line segment (when the three eigenvalues are colinear on the complex plane) or a single point (when the three eigenvalues overlap). It is additionally important to note that Theorem 1 is of particular relevance to the PolInSAR equal optimal scattering mechanism hypothesis [19], or otherwise referred to as *interferometrically polarimetric stationarity (IPS)* hypothesis [27]. It can be proved that for IPS to hold, $\tilde{\Omega}_{12}$ has to be normal. In the following sections, we will further exploit such a special property from the perspective of generic PolInSAR scattering models. We will show that these models indeed enjoy normality (hence fulfill IPS) and the shape of the coherence region is essentially determined by the number of phase centers within the resolution cell. Such fact consequently motivates the best normal matrix approximation solution for model inversion when dealing with measured data.

III. COHERENCE MODELING AND INVERSION: THE SINGLE PHASE CENTER CASE

A. Data Model

In this section, we consider the case where the resolution cell only contains a single phase center. Mostly this is characterized as flat surface scattering [10]. Single scattering phase center can also happen in the presence of dense vegetation when the radar cannot "see" through to the ground [28]. To be more precise, whenever the scatterer does not have distinctive vertical distributions or polarizations, the single-phase center applies. In such cases, the PolInSAR data can be modeled as:

$$\bar{\mathbf{T}} = \mathbf{T}_1, \quad (8)$$

$$\bar{\Omega}_{12} = \gamma_1 \mathbf{T}_1, \quad (9)$$

where \mathbf{T}_1 is the coherency matrix of the target and $\gamma_1 = \rho_1 e^{j\phi_1}$ is the corresponding complex coherence. The overbar for the terms on the left hand side of (8) and (9) indicates the modeled case where there is no finite multilooking effect. In real scenarios, one may expect \mathbf{T}_1 to represent an extended Bragg scatterer [5]. It is also possible that \mathbf{T}_1 comes purely from a uniformly distributed volume layer [2]. In such case, since each volume scatterer equally contributes to the backscatter, the net effect amounts to an averaged phase center lying at the middle of that layer.

Throughout this paper we always assume that $\bar{\mathbf{T}}^{-1}$ exists such that according to (8) and (9), the modeled whitened interferometric cross-correlation matrix becomes:

$$\bar{\tilde{\Omega}}_{12} = \bar{\mathbf{T}}^{-\frac{1}{2}} \bar{\Omega}_{12} \bar{\mathbf{T}}^{-\frac{1}{2}} = \gamma_1 \mathbf{I}_3, \quad (10)$$

where \mathbf{I}_3 is the 3×3 identity matrix. From the above equation it is clear that $\bar{\tilde{\Omega}}_{12}$ is a special normal matrix whose three eigenvalues are all equal to γ_1 . As a result, the numerical range of $\bar{\tilde{\Omega}}_{12}$, or equivalently, the coherence region, collapses to a single point on the complex plane where γ_1 exactly lies.

B. Best Normal Matrix Approximation Solution for Model Inversion

When dealing with measured data, the finite multilooking effect deteriorates the normality of the observed whitened interferometric cross-correlation matrix $\tilde{\Omega}_{12}$. Alternatively, this means that the observed coherence region will no longer be a single point but take up an extended area on the complex plane. In this case, we attempt to obtain the best approximation matrix to $\tilde{\Omega}_{12}$ that maintains the normality as the solution to model inversion. In light of (10), the optimization problem can be formulated by:

$$\begin{aligned} & \underset{\hat{\tilde{\Omega}}_{12}}{\text{minimize}} && \left\| \hat{\tilde{\Omega}}_{12} - \tilde{\Omega}_{12} \right\|_{\text{F}} \\ & \text{subject to} && \hat{\tilde{\Omega}}_{12} = \gamma_1 \mathbf{I}_3, \end{aligned} \quad (11)$$

where the subscript F stands for the Frobenius norm. For any complex matrix \mathbf{A} : $\|\mathbf{A}\|_{\text{F}}^2 = \text{Tr}(\mathbf{A}\mathbf{A}^{\text{H}})$ where $\text{Tr}(\cdot)$ represents the trace of a matrix. Note that (11) is a single complex variable optimization problem with regard to γ_1 which can be easily solved. In fact, we can re-write the minimizer in (11) as

$$\begin{aligned} \Delta &= \left\| \gamma_1 \mathbf{I}_3 - \tilde{\Omega}_{12} \right\|_{\text{F}}^2 \\ &= \text{Tr} \left(|\gamma_1|^2 \mathbf{I}_3 - \gamma_1 \tilde{\Omega}_{12}^{\text{H}} - \gamma_1^* \tilde{\Omega}_{12} + \tilde{\Omega}_{12} \tilde{\Omega}_{12}^{\text{H}} \right). \end{aligned} \quad (12)$$

Taking $\frac{\partial \Delta}{\partial \gamma_1} = 0$, the solution is given by:

$$\hat{\gamma}_1 = \frac{1}{3} \text{Tr} \left(\tilde{\Omega}_{12} \right). \quad (13)$$

As observed, (13) indicates that $\hat{\gamma}_1$ is the mean of the three eigenvalues of $\tilde{\Omega}_{12}$. From a geometrical point of view, $\hat{\gamma}_1$ lies at the centroid of the triangle formed by the eigenvalues of $\tilde{\Omega}_{12}$ in the complex plane. Consequently, the best normal matrix approximation to $\tilde{\Omega}_{12}$ in the case of one phase center is given by:

$$\hat{\tilde{\Omega}}_{12} = \frac{1}{3} \text{Tr} \left(\tilde{\Omega}_{12} \right) \mathbf{I}_3. \quad (14)$$

IV. COHERENCE MODELING AND INVERSION: THE DOUBLE PHASE CENTER CASE

A. Data Model

In this section, we consider the second case where the resolution cell contains two different phase centers. The scattering model can be written as:

$$\bar{\mathbf{T}} = \mathbf{T}_1 + \mathbf{T}_2, \quad (15)$$

$$\bar{\Omega}_{12} = \gamma_1 \mathbf{T}_1 + \gamma_2 \mathbf{T}_2, \quad (16)$$

where \mathbf{T}_i is the polarimetric coherency matrix and $\gamma_i = \rho_i e^{j\phi_i}$ is the complex coherence associated with either target. It is worth emphasizing that (15) and (16) contain the specific case of the RVoG model where \mathbf{T}_1 may represent the localized scatterer on the ground and \mathbf{T}_2 represents the volume layer overhead. Assuming no temporal and baseline decorrelation, $\gamma_1 = e^{j\phi_1}$ codes the ground phase whereas the volume coherence $\gamma_2 = \rho_2 e^{j\phi_2}$ accounts for both the propagation

extinction (ρ_2) and the averaged scattering center (ϕ_2) of the vegetation layer.

According to (15) and (16), the modeled interferometric coherence is:

$$\bar{\gamma}(\mathbf{w}) = \gamma_2 + \frac{\mu(\mathbf{w})}{1 + \mu(\mathbf{w})}(\gamma_1 - \gamma_2), \quad (17)$$

where

$$\mu(\mathbf{w}) = \frac{\mathbf{w}^H \mathbf{T}_1 \mathbf{w}}{\mathbf{w}^H \mathbf{T}_2 \mathbf{w}}. \quad (18)$$

As observed, the coherence region defined by (17) delineates a line on the complex plane. In other words, the numerical range of $\bar{\tilde{\Omega}}_{12} = \bar{\mathbf{T}}^{-\frac{1}{2}} \bar{\tilde{\Omega}}_{12} \bar{\mathbf{T}}^{-\frac{1}{2}}$ is a line segment. This evidence consequently dictates that $\bar{\tilde{\Omega}}_{12}$ be a normal matrix according to the following theorem [29]:

Theorem 2. *If $W(\mathbf{A})$ is a line segment, \mathbf{A} is normal.*

Note that Theorem 2 can be regarded as a special case of Theorem 1 and its application to the study of RVoG model was first introduced by Neumann et al. in [30].

B. Best Normal Matrix Approximation Solution for Model Inversion

Again, in the measured case, $\tilde{\Omega}_{12}$ is unlikely to be normal but we can invert a normal matrix that is closest to $\tilde{\Omega}_{12}$ in the sense of minimum norm. However, what complicates the problem in this case is that we need to further constrain the numerical range to be a line segment. To be specific, the optimization must be formulated as follows:

$$\underset{\hat{\tilde{\Omega}}_{12}}{\text{minimize}} \quad \left\| \hat{\tilde{\Omega}}_{12} - \tilde{\Omega}_{12} \right\|_{\text{F}} \quad (19)$$

subject to $W(\hat{\tilde{\Omega}}_{12})$ is a line segment.

In order to solve the aforementioned problem, we first invoke the following theorem [25]:

Theorem 3. *The numerical range $W(\mathbf{A})$ of a matrix \mathbf{A} is a line segment exactly when \mathbf{A} and a Hermitian matrix are affine equivalents. That is, there exist some $a, c \in \mathbb{C}$ and a Hermitian matrix \mathbf{B} such that $\mathbf{A} = a\mathbf{B} + c\mathbf{I}$.*

As a consequence of Theorem 2, (19) can be reformulated as:

$$\underset{a, c, \mathbf{B}}{\text{minimize}} \quad \left\| (a\mathbf{B} + c\mathbf{I}_3) - \tilde{\Omega}_{12} \right\|_{\text{F}} \quad (20)$$

subject to $\mathbf{B} = \mathbf{B}^H$.

Excitingly, the above optimization problem is analytically tractable. We provide the derivation in Appendix A. Algorithm 1 summarizes the procedure for obtaining the best normal matrix approximation to $\tilde{\Omega}_{12}$.

As an additional remark, we note the difference between the method proposed here and a recent work by Lopez-Martinez et al. in [20] where a normal matrix approximation $\hat{\tilde{\Omega}}_{12}$ is also derived. These two optimization methods lead to different solutions. Specifically, [20] is based on minimizing the skew-Hermitian part of the affine transformation of $\tilde{\Omega}_{12}$ such that $\hat{\tilde{\Omega}}_{12}$ is computed by the corresponding

inverse affine transformation after discarding the minimized skew-Hermitian matrix. Consequently, it does not necessarily minimize $\|\tilde{\Omega}_{12} - \hat{\tilde{\Omega}}_{12}\|_{\text{F}}^2$ (see Table I in Section VII-B), in other words, it is not the *best* normal matrix approximation solution. On the other hand, the proposed method does not make explicit use of the affine transformation but directly solve the best normal matrix approximation problem (19) or (20), which guarantees the minimization of $\|\tilde{\Omega}_{12} - \hat{\tilde{\Omega}}_{12}\|_{\text{F}}^2$. More importantly, this property of the solution subsequently motivates a simple and effective way for model validation using only the minimized norm (see Section IV) contrary to [20]. Indeed, a more sophisticated method based on maximum likelihood test is proposed in [20] for model validation instead.

Algorithm 1

input: $\tilde{\Omega}_{12}$

$$\begin{aligned} \mathbf{H}_1 &= \left(\tilde{\Omega}_{12} + \tilde{\Omega}_{12}^H \right) / 2, \mathbf{H}_2 = \left(\tilde{\Omega}_{12} - \tilde{\Omega}_{12}^H \right) / (2j), \\ A &= 4 \text{Tr}(\mathbf{H}_1^2), B = -8 \text{Tr}(\mathbf{H}_1 \mathbf{H}_2), C = 4 \text{Tr}(\mathbf{H}_2^2) \\ D &= 4 \text{Tr}(\mathbf{H}_1), E = -4 \text{Tr}(\mathbf{H}_2), F = 3, \\ X &= (4AF - D^2 - 4CF + E^2) / 2, Y = 2BF - DE \\ \theta &= [\text{atan2}(Y, X) + \pi] / 2 \\ \rho &= -2F / (D \cos \theta + E \sin \theta) \\ z &= \rho (\cos \theta + j \sin \theta) \\ \hat{\tilde{\Omega}}_{12} &= \left(z \tilde{\Omega}_{12} - z^* \tilde{\Omega}_{12}^H - \mathbf{I} \right) / (2z) \end{aligned}$$

output: $\hat{\tilde{\Omega}}_{12}$

V. COHERENCE MODELING AND INVERSION: THE TRIPLE PHASE CENTER CASE

A. Data Model

In this section, we investigate the third case when the resolution contains three different phase centers. Similarly, the scattering model is:

$$\bar{\mathbf{T}} = \sum_{i=1}^3 \mathbf{T}_i, \quad (21)$$

$$\bar{\tilde{\Omega}}_{12} = \sum_{i=1}^3 \gamma_i \mathbf{T}_i. \quad (22)$$

We have already seen in Section III that when the resolution cell contains a single phase center, the modeled whitened interferometric cross-correlation matrix is a normal matrix whose numerical range (coherence region) contracts to one point on the complex. On the other hand, Section IV tells us that in the case of two phase centers, the modeled whitened matrix is also normal whose numerical range becomes a line segment. In particular, (10) and Theorem 2 respectively guarantee the normality for these two situations for any $\gamma_i \in \mathbb{C}$, no matter what \mathbf{T}_i look like. This, unfortunately, is not the case for the triple phase center model. One may verify that for arbitrarily chosen \mathbf{T}_i in (21)–(22), $\bar{\tilde{\Omega}}_{12} = \bar{\mathbf{T}}^{-\frac{1}{2}} \bar{\tilde{\Omega}}_{12} \bar{\mathbf{T}}^{-\frac{1}{2}}$ is not always normal. It then follows that for $\bar{\tilde{\Omega}}_{12}$ to be normal $\forall \gamma_i$, \mathbf{T}_i must satisfy the following condition:

$$\mathbf{T}_i \bar{\mathbf{T}}^{-1} \mathbf{T}_j = \mathbf{T}_j \bar{\mathbf{T}}^{-1} \mathbf{T}_i, i \neq j, i, j = 1, 2, 3, \quad (23)$$

where $\bar{\mathbf{T}}$ is given by (21). The proof is provided Appendix B. It should be noted that (23) is redundant. As a matter of fact, we only need to verify one pair of $i \neq j$ according to Lemma 1 in Appendix B.

However, (23) is non-constructive. It does not provide much insight as to what \mathbf{T}_i could each look like in order to fulfill the normality, a point that deserves further investigation. Indeed, it seems that the discussion is *ad hoc* and at this stage we have not been able to exhaust all the possible structures of \mathbf{T}_i except for some limited cases. Among them, there exists a very interesting one. It turns out that if \mathbf{T}_i are all single-rank matrices (single-scatterers), that is, if (21) and (22) can be written as:

$$\bar{\mathbf{T}} = \sum_{i=1}^3 \mathbf{k}_i \mathbf{k}_i^H, \quad (24)$$

$$\bar{\Omega}_{12} = \sum_{i=1}^3 \gamma_i \mathbf{k}_i \mathbf{k}_i^H. \quad (25)$$

then $\bar{\Omega}_{12} = \bar{\mathbf{T}}^{-\frac{1}{2}} \bar{\Omega}_{12} \bar{\mathbf{T}}^{-\frac{1}{2}}$ is normal. This can be proved via validation of (23) and is left for interested readers (hint: $\mathbf{k}_i^H \bar{\mathbf{T}}^{-1} \mathbf{k}_j = 0$ for $i \neq j$). Nonetheless, in the following we provide an alternative proof which reveals the intrinsic relationship between the coherence of each scatterer and the eigenvalues of $\bar{\Omega}_{12}$. In particular, we have the following theorem:

Theorem 4. $\bar{\Omega}_{12} = \bar{\mathbf{T}}^{-\frac{1}{2}} \bar{\Omega}_{12} \bar{\mathbf{T}}^{-\frac{1}{2}}$ is normal if and only if $\bar{\mathbf{T}}$ and $\bar{\Omega}_{12}$ can be respectively written by (24) and (25).

Proof. We first prove the sufficient condition. Note that (24)–(25) can be re-written in the more compact form by:

$$\bar{\mathbf{T}} = \mathbf{K} \mathbf{K}^H, \quad (26)$$

$$\bar{\Omega}_{12} = \mathbf{K} \mathbf{\Gamma} \mathbf{K}^H, \quad (27)$$

where $\mathbf{K} = [\mathbf{k}_1, \mathbf{k}_2, \mathbf{k}_3]$ and $\mathbf{\Gamma} = \text{diag}(\gamma_1, \gamma_2, \gamma_3)$. Then we define the 3×3 matrix \mathbf{U} by:

$$\mathbf{U} = \bar{\mathbf{T}}^{-\frac{1}{2}} \mathbf{K}. \quad (28)$$

It is easy to verify that \mathbf{U} is unitary. In fact, according to (26) and (28) we have:

$$\mathbf{U} \mathbf{U}^H = \bar{\mathbf{T}}^{-\frac{1}{2}} \mathbf{K} \mathbf{K}^H \bar{\mathbf{T}}^{-\frac{1}{2}} = \mathbf{I}. \quad (29)$$

Thus by (27) $\bar{\Omega}_{12}$ can be written as:

$$\bar{\Omega}_{12} = \bar{\mathbf{T}}^{-\frac{1}{2}} \mathbf{K} \mathbf{\Gamma} \mathbf{K}^H \bar{\mathbf{T}}^{-\frac{1}{2}} = \mathbf{U} \mathbf{\Gamma} \mathbf{U}^H. \quad (30)$$

(30) says that $\bar{\Omega}_{12}$ is diagonalizable to $\mathbf{\Gamma}$ by the unitary matrix \mathbf{U} and hence by the definition of matrix normality, the theorem holds.

Next we prove the necessary condition. Since $\bar{\Omega}_{12} = \bar{\mathbf{T}}^{-\frac{1}{2}} \bar{\Omega}_{12} \bar{\mathbf{T}}^{-\frac{1}{2}}$ is normal, it is unitarily diagonalizable:

$$\bar{\Omega}_{12} = \bar{\mathbf{T}}^{-\frac{1}{2}} \bar{\Omega}_{12} \bar{\mathbf{T}}^{-\frac{1}{2}} = \mathbf{U} \mathbf{\Gamma} \mathbf{U}^H, \quad (31)$$

such that

$$\bar{\Omega}_{12} = \bar{\mathbf{T}}^{-\frac{1}{2}} \mathbf{U} \mathbf{\Gamma} \mathbf{U}^H \bar{\mathbf{T}}^{-\frac{1}{2}}. \quad (32)$$

Let $\mathbf{K} = \bar{\mathbf{T}}^{-\frac{1}{2}} \mathbf{U}$, then (32) becomes:

$$\bar{\Omega}_{12} = \mathbf{K} \mathbf{\Gamma} \mathbf{K}, \quad (33)$$

and

$$\bar{\mathbf{T}} = \bar{\mathbf{T}}^{-\frac{1}{2}} \left(\bar{\mathbf{T}}^{-\frac{1}{2}} \right)^H = \mathbf{K} \mathbf{U} \mathbf{U}^H \mathbf{K}^H = \mathbf{K} \mathbf{K}^H. \quad (34)$$

By (33) and (34), the theorem holds. \square

Essentially, Theorem 4 says that if the resolution cell does physically consist of three single scatterers, their respective complex coherences can be conveniently obtained through eigendecomposition of $\bar{\Omega}_{12}$. Note that this imposes a strong restriction on the scattering scenario, which is indeed reported in a controlled experiment in anechoic chamber by Colin et al. [16]. However, even if \mathbf{T}_i are not single-rank, Theorem 4 also says as long as $\bar{\Omega}_{12}$ is normal, the resolution cell can be always *decomposed* (at least conceptually) into three single-scatterers whose associated complex coherences respectively correspond to the vertices of the triangular coherence region. This is a very important property revealed from the normality/IPS assumption and can be even considered as a PolInSAR parallel to the PolSAR H/ α decomposition [8]. However, contrary to PolSAR, the three single-scatterers in the PolInSAR decomposition are not necessarily orthogonal to each other. In the next subsection, we will see how it applies to the single and double phase center cases to provide an alternative interpretation of those two models.

B. Link to Single and Double Phase Center Models

Here we show that the single and double phase center models, with their whitened interferometric cross-correlation matrices being both normal, can be also expressed as sum of three single scatterers.

For the single phase center case, we only need to replace \mathbf{T}_1 in (8) and (9) with its eigendecomposition and the scattering model becomes:

$$\bar{\mathbf{T}} = \sum_{i=1}^3 \lambda_i \mathbf{v}_i \mathbf{v}_i^H, \quad (35)$$

$$\bar{\Omega}_{12} = \sum_{i=1}^3 \gamma_i (\lambda_i \mathbf{v}_i \mathbf{v}_i^H), \quad (36)$$

where λ_i are the eigenvalues and \mathbf{v}_i are the corresponding eigenvectors. Thus by comparing with (24) and (25), one immediately sees that $\mathbf{k}_i = \sqrt{\lambda_i} \mathbf{v}_i$ and $\gamma'_i = \gamma_i$, meaning that the coherences of all scatterers are equal.

For the double phase center model, we rewrite (15) as:

$$\bar{\mathbf{T}} = \mathbf{T}_2^{\frac{1}{2}} \left(\mathbf{T}_2^{-\frac{1}{2}} \mathbf{T}_1 \mathbf{T}_2^{-\frac{1}{2}} + \mathbf{I} \right) \mathbf{T}_2^{\frac{1}{2}}. \quad (37)$$

Then suppose the eigendecomposition of $\mathbf{T}_2^{-\frac{1}{2}} \mathbf{T}_1 \mathbf{T}_2^{-\frac{1}{2}}$ is given by $\mathbf{T}_2^{-\frac{1}{2}} \mathbf{T}_1 \mathbf{T}_2^{-\frac{1}{2}} = \sum_{i=1}^3 \lambda_i \mathbf{v}_i \mathbf{v}_i^H$ and also notice $\mathbf{I} = \sum_{i=1}^3 \mathbf{v}_i \mathbf{v}_i^H$, the above equation becomes:

$$\bar{\mathbf{T}} = \sum_{i=1}^3 (\lambda_i + 1) \left(\mathbf{T}_2^{-\frac{1}{2}} \mathbf{v}_i \right) \left(\mathbf{T}_2^{-\frac{1}{2}} \mathbf{v}_i \right)^H. \quad (38)$$

Similarly, (16) can be written as:

$$\bar{\mathbf{\Omega}}_{12} = \sum_{i=1}^3 (\lambda_i \gamma_1 + \gamma_2) \left(\mathbf{T}_2^{-\frac{1}{2}} \mathbf{v}_i \right) \left(\mathbf{T}_2^{-\frac{1}{2}} \mathbf{v}_i \right)^H. \quad (39)$$

Thus by comparing with (24) and (25), one sees that $\mathbf{k}_i = \sqrt{\lambda_i + 1} \mathbf{T}_2^{-\frac{1}{2}} \mathbf{v}_i$ and $\gamma'_i = \frac{\lambda_i}{\lambda_i + 1} \gamma_1 + \frac{1}{\lambda_i + 1} \gamma_2$. The latter result shows that the coherences of the three single scatterers are colinear between the line segment with γ_1 and γ_2 as the end points.

Therefore, the single phase center and double phase center models can be also regarded as containing three single scatterers except that for the former all their coherences are equal whereas for the latter the coherences are linearly aligned. The significance is that the three models introduced so far constitute a hierarchical way of describing the PolInSAR scattering mechanism. If one model cannot properly fit the data, increasing the model order guarantees to improve the result. For details, see also Section VI.

C. Best Normal Matrix Approximation Solution for Model Inversion

Once again, as can be expected, the measured whitened interferometric cross-correlation matrix $\tilde{\mathbf{\Omega}}_{12}$ will be no longer normal due to finite multilook averaging. In this case, we still attempt to estimate a normal matrix $\hat{\mathbf{\Omega}}_{12}$ that is closest to $\tilde{\mathbf{\Omega}}_{12}$. Specifically, now we need to solve the following optimization:

$$\begin{aligned} & \underset{\hat{\mathbf{\Omega}}_{12}}{\text{minimize}} \quad \left\| \hat{\mathbf{\Omega}}_{12} - \tilde{\mathbf{\Omega}}_{12} \right\|_F \\ & \text{subject to} \quad \hat{\mathbf{\Omega}}_{12}^H \hat{\mathbf{\Omega}}_{12} = \hat{\mathbf{\Omega}}_{12} \hat{\mathbf{\Omega}}_{12}^H. \end{aligned} \quad (40)$$

As a matter of fact, (40) poses the best normal matrix approximation problem in the most general form, which has been perfectly solved by Ruhe [31]. He showed that finding the closest normal matrix is equivalent to finding the unitary similarity transformation which maximizes the diagonal elements and for this purpose the Jacobian algorithm is readily designed (an online MATLAB code is provided at [32]). Very interestingly, the Jacobian algorithm has been also applied by Ferro-Famil et al [19] whereas their purpose, as differed from here, is to use it for line segment estimation of the RVoG model. However, as we have seen, the best normal matrix approximation solution itself has a clear physical explanation by which the eigen spectrum directly corresponds to the interferometric phase of each single scatterer. From a geometrical point of view, (40) attempts to approximate the numerical range of $\tilde{\mathbf{\Omega}}_{12}$ with a triangle whose vertices are the three eigenvalues of $\tilde{\mathbf{\Omega}}_{12}$ (according to Theorem 1). Suppose the Jacobian decomposition of $\tilde{\mathbf{\Omega}}_{12}$ is:

$$\tilde{\mathbf{\Omega}}_{12} = \mathbf{U} \mathbf{\Gamma} \mathbf{U}^H. \quad (41)$$

Then the best normal matrix approximation to $\tilde{\mathbf{\Omega}}_{12}$ is given by:

$$\hat{\mathbf{\Omega}}_{12} = \mathbf{U} \text{diag}(\mathbf{\Gamma}) \mathbf{U}^H, \quad (42)$$

where $\text{diag}(\mathbf{\Gamma})$ denotes the diagonal matrix consisting of the diagonal elements of $\mathbf{\Gamma}$.

VI. VALIDATION OF SCATTERING MODELS

In practice, it is seldom possible to know a priori the true number of phase centers within a resolution cell. It is thus desirable to devise a way to validate the aforementioned scattering models. For doing so, we can calculate the relative error between the observed whitened interferometric cross-correlation matrix and its best normal approximation as follows:

$$\delta = \frac{\left\| \hat{\mathbf{\Omega}}_{12} - \tilde{\mathbf{\Omega}}_{12} \right\|_F^2}{\left\| \tilde{\mathbf{\Omega}}_{12} \right\|_F^2}. \quad (43)$$

Since $\hat{\mathbf{\Omega}}_{12}$ is the closest normal matrix to $\tilde{\mathbf{\Omega}}_{12}$, δ is the smallest relative error possible when assuming the given model. If δ is small, we may accept the model whereas if its value remains large, it is likely that the model does not apply. Since we have an hierarchy of models to describe the PolInSAR data, it is always possible to decrease the relative error by increasing the assumed number of phase centers. Then starting from the single phase center model, this process stops if (43) is sufficiently small (meaning model is accepted).

However, it is important to realize that the validation so implemented is limited by the normality assumption. We have seen that the normality of the whitened interferometric cross-correlation matrix is maintained if the resolution cell contains no more than three phase centers. When the resolution cell contains more than three phase centers or even when there are only three phase centers but the normality does not hold, the best normal approximation solution is not meaningful anymore. In both cases, we may expect a large δ whatsoever. We remark that such limitation is an indicator of the maximum number of phase centers that a single-baseline PolInSAR dataset can discriminate. Note that this is independent of the method used because of the limited information contained therein. In fact, Colin et al. [16] has pointed out that their proposed coherence optimization method cannot distinguish more than three single scatterers, either. From the ESPRIT approach perspective [21], three is also the maximum number of sources discriminable given only three independent polarization channels (i.e., HH, HV, and VV).

Last, it is worth noting that (43) does not rely on any specific distribution assumption nor it is dependent on scattering power (because $\tilde{\mathbf{\Omega}}_{12}$ is whitened). Validity test of the scattering models is generic for different PolInSAR datasets.

VII. SIMULATION

We provide the simulation results of coherence estimation based on the scattering models in Section III, IV, and V. The observed \mathbf{T}_6 matrices are all randomly generated from the scattering models with multilook processing. That is, if $\bar{\mathbf{T}}_6$ is the modeled PolInSAR coherency matrix, the observed matrix is simulated by:

$$\mathbf{T}_6 = \bar{\mathbf{T}}_6^{\frac{1}{2}} \left(\frac{1}{L} \sum_{l=1}^L \mathbf{u}_l \mathbf{u}_l^H \right) \bar{\mathbf{T}}_6^{\frac{1}{2}}, \quad (44)$$

where \mathbf{u}_i are independent Gaussian vectors of zero mean and unit covariance matrix. L is the number of looks. Throughout this section, $L = 100$ is used.

A. Results of Single Phase Center Case

For the single phase center case, we hypothesize an extended Bragg scatterer. The polarimetric coherence matrix is given by [5]:

$$\overline{\mathbf{T}} = \begin{bmatrix} C_1 & C_2 \text{sinc}(2\beta) & 0 \\ C_2^* \text{sinc}(2\beta) & C_3[1 + \text{sinc}(4\beta)] & 0 \\ 0 & 0 & C_3[1 - \text{sinc}(4\beta)] \end{bmatrix}. \quad (45)$$

In this paper $C_1 = 1, C_2 = 0.2 + 0.2j, C_3 = 0.5, \beta = 0.05\pi$ are adopted. Additionally, the interferometric cross-correlation matrix is given by:

$$\overline{\Omega} = 0.9e^{j0.5\pi}\overline{\mathbf{T}}. \quad (46)$$

Fig. 1 shows the boundary of the observed coherence region (blue broken line), the true coherence region (black asterisk), as well as the estimated coherence region (red asterisk) according to (13). As expected, the observed coherence region is not a single point but an extended area due to the finite multilooking effect. The best normal approximation solution, on the other hand, provides a meaningful estimation that is close to its true position. For the current example, the estimated coherence is $\hat{\gamma} = 0.88e^{j0.50\pi}$ which is a very good approximation to the true value of $0.9e^{j0.5\pi}$.

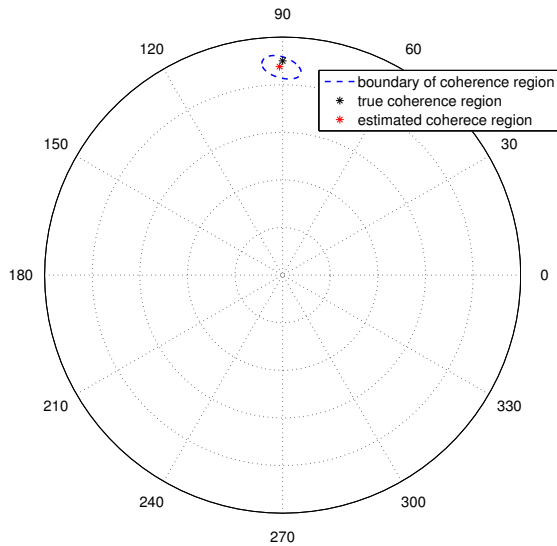


Fig. 1. Coherence estimation result for the simulated single phase center data by the proposed method. In this case, the true coherence region is a single point and equal to $0.9e^{j0.5\pi}$.

B. Results of Double Phase Center Case

For the double phase center case, we assume the scattering model to be composed of a localized ground scatterer overlaid

by a vegetation layer (i.e., the RVoG model). Specifically, the polarimetric coherence matrix as well as the interferometric cross-correlation matrix are respectively given by:

$$\overline{\mathbf{T}} = \mathbf{T}_g + \mathbf{T}_v, \quad (47)$$

$$\overline{\Omega} = 0.9e^{j\frac{\pi}{2}}\mathbf{T}_g + 0.3e^{j\frac{\pi}{5}}\mathbf{T}_v, \quad (48)$$

where the ground scatterer \mathbf{T}_g is again assumed to be an extended Bragg scatterer and the volume scattering model is given by [9]:

$$\mathbf{T}_v = \begin{bmatrix} 2 & 0 & 0 \\ 0 & 1 & 0 \\ 0 & 0 & 1 \end{bmatrix}. \quad (49)$$

Coherence estimation of the RVoG model is performed by three methods, i.e., Algorithm 1 (proposed), the coherence extrema estimation method [19], as well as the affine transformation (AT) based method [20], given that the latter two are also able to produce line segment approximation. Fig. 2 shows the results. It can be seen that proposed method seems superior in terms of the closest proximity to the true coherence region. To confirm this claim, we evaluate the relative error of the result by:

$$\delta_1 = \frac{\sum_{i=1}^2 |\hat{z}_i - z_i|^2}{\sum_{i=1}^3 |z_i|^2}, \quad (50)$$

where z_1 and z_2 are the end points of the true line segment while \hat{z}_1 and \hat{z}_2 are those of the estimated one. The average value of δ_1 in 2000 independent simulations is given in Table II. One sees that the proposed method achieves the best performance, seconded by the coherence extrema method, and by the AT method. We also make special note to the large error of the AT method, which is possibly attributed to its trend to "overshoot" the coherence region as is clear from Fig. 2(c). Nonetheless, its accuracy is quite good if only in terms of the slope estimation. Table I lists the slope and intercept of each line segment in Fig. 2. One can see that the proposed method performs similarly to (in this case slightly better than) the AT method, whereas both of them considerably outperform the coherence extrema method.

Another interesting comparison can be done between the proposed algorithm and the AT method because both of them are able to directly estimate the whitened interferometric cross-correlation matrix. In this case, we can calculate the relative error by:

$$\delta_2 = \frac{\|\hat{\tilde{\Omega}}_{12} - \tilde{\tilde{\Omega}}_{12}\|_F^2}{\|\tilde{\tilde{\Omega}}_{12}\|_F^2}, \quad (51)$$

where $\tilde{\tilde{\Omega}}_{12}$ is the true matrix and $\hat{\tilde{\Omega}}_{12}$ is the estimated version. The average value of δ_2 in 1000 independent simulations is given in Table II as well, where the proposed method again shows better result. As previously mentioned in Section IV-B, this should have been expected since the AT method also derives a normal matrix $\hat{\tilde{\Omega}}_{12}$ but the approximation principle is based on minimizing the skew-Hermitian part of the affine transformation of $\tilde{\tilde{\Omega}}_{12}$. It does not minimize $\|\hat{\tilde{\Omega}}_{12} - \tilde{\tilde{\Omega}}_{12}\|_F^2$ nor $\|\hat{\tilde{\Omega}}_{12} - \tilde{\tilde{\Omega}}_{12}\|_F^2$, if from the statistical average point of view. On

the other hand, Algorithm 1 directly solves the optimization problem (19) and hence guarantees to minimize the distance among all the possible normal matrix solutions.

TABLE I
LINE SLOPE (k) AND INTERCEPT (b) RESULTS OF FIG. 2 BY PROPOSED METHOD, COHERENCE EXTREMA ESTIMATION METHOD [19], AND AT METHOD [20]

	True	Proposed	Extrema Estimation	AT
k	3.217	3.783	0.874	3.980
b	-0.742	-0.923	-0.124	-0.995

TABLE II
COHERENCE INVERSION ACCURACY OF SIMULATED DOUBLE PHASE CENTER DATA BY PROPOSED METHOD, COHERENCE EXTREMA ESTIMATION METHOD [19], AND AT METHOD [20]. AVERAGE VALUES PER 2000 INDEPENDENT EXPERIMENTS ARE REPORTED

	Proposed	Extrema Estimation	AT
δ_1	0.1631	0.2815	687.5
δ_2	0.3653	N/A	717.8

C. Results of Triple Phase Center Case

In this subsection, we provide the simulation results for the case when the resolution cell contains three single-scatterers with different phase centers. According to the anechoic chamber measurements reported in [16], the typical Pauli-vectors of such configuration can be expressed as:

$$\mathbf{K} = [\mathbf{k}_1, \mathbf{k}_2, \mathbf{k}_3] = \begin{bmatrix} \epsilon & 0.9 & 0.9 \\ 1 & \alpha e^{j1.8} & 0.3 \\ \epsilon & \epsilon & \epsilon \end{bmatrix}, \quad (52)$$

where $\epsilon = 0.05$ and $\alpha = 0.3$ are chosen here. In addition, the coherences of each scatterer are assumed to be:

$$\mathbf{\Gamma} = \begin{bmatrix} |\gamma|e^{j\frac{\pi}{10}} & 0 & 0 \\ 0 & |\gamma|e^{j\frac{\pi}{3}} & 0 \\ 0 & 0 & |\gamma|e^{-j\frac{\pi}{3}} \end{bmatrix}, \quad (53)$$

where $|\gamma|$ is the coherence magnitude level. In our simulation $|\gamma|$ takes four different values: 0.90, 0.93, 0.96, 0.99. Note that they are all close to 1 so as to emulate the anechoic chamber measurement of well separated scatterers in low noise environment. In this case, only estimation of interferometric phases is relevant and three methods are compared for their performances in phase estimation: 1) the proposed method (Jacobian algorithm), 2) the coherence optimization approach by Colin et al. [16], and 3) the ESPRIT algorithm [21], [23]. The estimation results for $|\gamma| = 0.96$ is displayed in Fig. 3. The accuracy of phase estimation will be further evaluated by:

$$\delta_3 = \frac{\sum_{i=1}^3 |\hat{\phi}_i - \phi_i|^2}{\sum_{i=1}^3 |\phi_i|^2}, \quad (54)$$

where ϕ_i and $\hat{\phi}_i$ are the true and estimated phases, respectively. Table III shows the average values of δ_3 of 2000 independent simulations. Interestingly, one sees that Colin's method achieves the best accuracy at high coherence levels while the proposed method becomes superior at lower $|\gamma|$. Both the methods, however, outperforms the ESPRIT method.

TABLE III
PHASE ESTIMATION ACCURACY OF SIMULATED TRIPLE PHASE CENTER DATA BY PROPOSED METHOD, COHERENCE OPTIMIZATION METHOD [16], AND ESPRIT ALGORITHM [21],[23]. AVERAGE VALUES PER 2000 INDEPENDENT EXPERIMENTS ARE REPORTED

$ \gamma $	Proposed	Coherence Optimization	ESPRIT
0.90	1.64×10^{-3}	1.87×10^{-3}	6.12×10^{-3}
0.93	1.11×10^{-3}	1.11×10^{-3}	4.32×10^{-3}
0.96	6.36×10^{-4}	5.74×10^{-4}	3.49×10^{-3}
0.99	2.01×10^{-4}	1.40×10^{-4}	3.39×10^{-3}

VIII. EXPERIMENTAL RESULTS USING REAL POLINSAR DATA

In this section, we provide the coherence estimation results for real PolInSAR data. The dataset was acquired in a repeat-pass mode by the L-band E-SAR system in the area of Oberpfaffenhofen of Germany. The spatial baseline is 15 meters and the temporal baseline is 10 minutes. In order to suppress the speckle and obtain a proper estimation of the \mathbf{T}_6 matrix, the dataset has been processed with a 2×2 spatial multilooking followed by the improved sigma filter [33]. As a result, the equivalent number of looks (ENL) has been increased to more than 100. The Pauli-display of master PolSAR image is shown in Fig. 4.

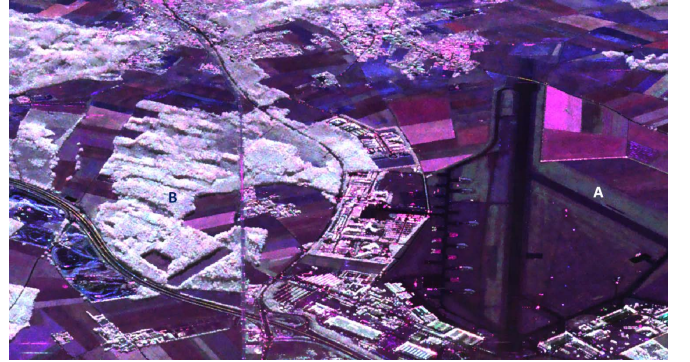


Fig. 4. Pauli-display of the E-SAR master polarimetric image. The PolInSAR data have been processed by 2×2 spatial multilooking followed by improved sigma filter.

First of all, one sees that the right part of Fig. 4 is mainly covered by flat ground. Thus it is expected that in such area only one phase center dominates. In order to verify this conjecture, we select one target as indicated by point A in Fig. 4 and plot its coherence region. The result is shown in Fig. 5, which clearly witnesses the concentration of the coherence region. In fact, the whitened correlation matrix of the selected scatterer is:

$$\tilde{\mathbf{\Omega}} = \begin{bmatrix} 0.854 - 0.416j & 0.023 - 0.032j & 0.004 + 0.013j \\ 0.003 + 0.008j & 0.809 - 0.449j & -0.018 + 0.009j \\ -0.016 + 0.020j & 0.014 - 0.013j & 0.849 - 0.450j \end{bmatrix}, \quad (55)$$

which can be well approximated by $\hat{\tilde{\mathbf{\Omega}}} = (0.837 - 0.438j) \times \mathbf{I}_3$ according to (13). By (43) the relative error in this case is only 0.38%. The relative error of the best normal matrix solution assuming single phase center for each pixel is shown in Fig. 6. By comparing with Fig. 4, one observes that the

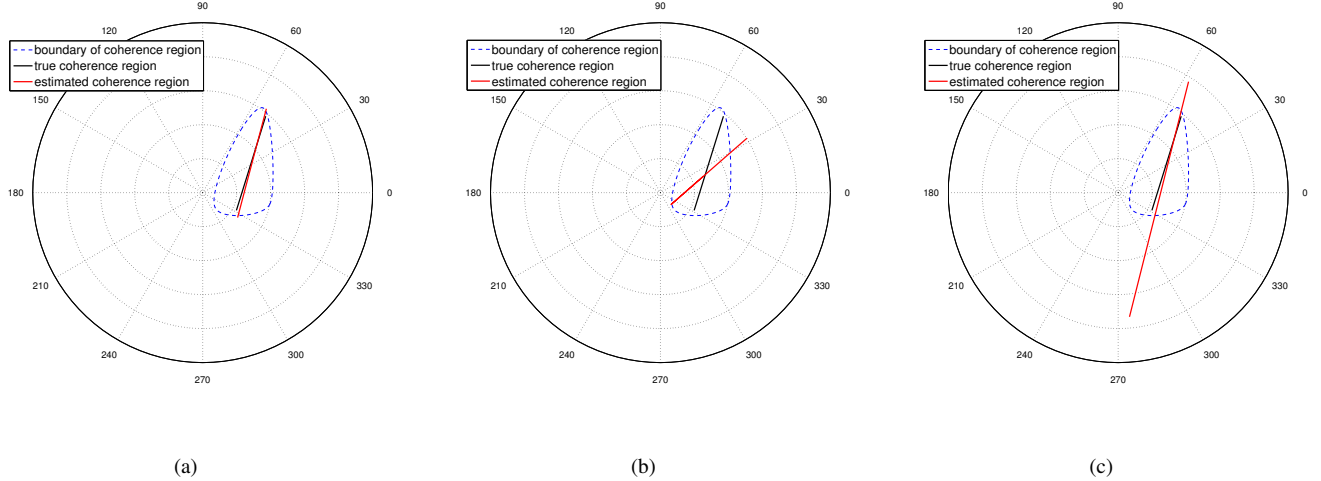


Fig. 2. Coherence estimation result for the simulated double phase center data by (a) proposed method (Algorithm 1), (b) coherence extrema estimation method [19], and (c) AT method [20]. The true coherence region is computed by the convex hull (in this case a line segment) of the eigenvalues of the true whitened interferometric cross-correlation matrix $\overline{\overline{\Omega}}_{12}$.

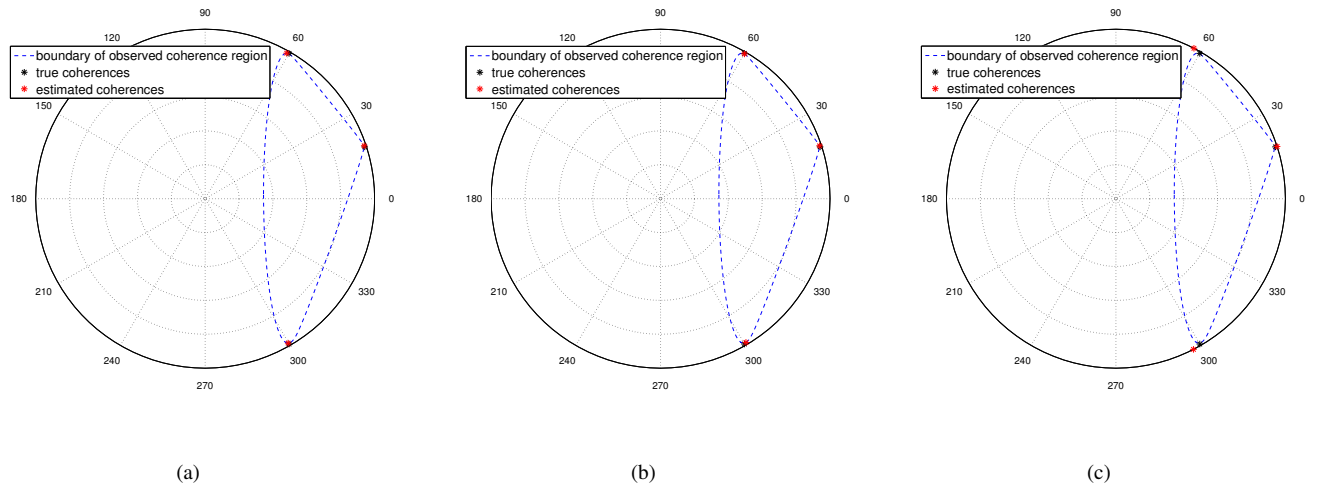


Fig. 3. Coherence estimation results for simulated triple phase center data by (a) proposed method (Jacobian algorithm), (b) coherence estimation method [16], and (c) ESPRIT algorithm [21], [23]. The true coherences are given by (53) where $|\gamma| = 0.96$.

approximation error in most of the surface scattering area is indeed very small, implying the validity of the single phase center assumption on the ground. The exception happens at the runway where the signal-to-noise ratio (SNR) is extremely low. The system thermal noise is playing a much significant role in such scenarios.

More importantly, Fig. 6 is an evident demonstration of the power of PolInSAR for it also informs which places cannot be properly characterized by single phase center scattering, a job not easily accomplished by conventional InSAR. Especially one sees that the relative approximation error appears quite large in much of the forest area. To show this clearly, the coherence region of a second target (marked as point B in Fig. 4) is plotted in Fig. 7, where an elongated shape can be observed. The single phase center approximation leads to a relative error as large as 23.7%. Instead, if we assume a double phase center scattering model, that is, if we approximate the

observed coherence region by a line segment according to Algorithm 1, the relative error will be significantly reduced to 2.2%. The estimated line segment is also plotted in Fig. 7, where one sees that the shape of the coherence region has been nicely caught. For a general appreciation of how the double phase center scattering model fits the real PolInSAR data, the relative error for each pixel is displayed in Fig. 8. This figure indicates that the relative errors of more than 80% of the pixels are smaller than 5%.

Nevertheless, one may observe a considerable number of pixels whose relative errors are still large in Fig. 8, particularly within the forest areas at the upper left of the scene. This fact implies that a double phase center model cannot properly fit the data. Therefore, in order to reduce the approximation error, we further approximate the observed whitened interferometric cross-correlation matrix by the Jacobian algorithm. The corresponding relative error for each pixel is shown in Fig. 9.

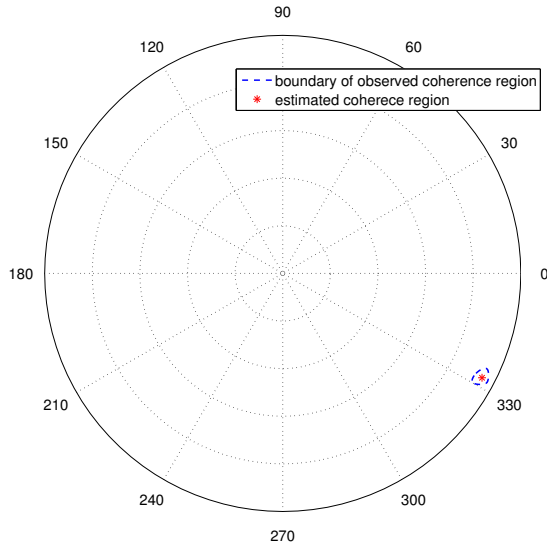


Fig. 5. Coherence estimation result for "target A" in Fig. 4 by best normal matrix approximation assuming single phase center.

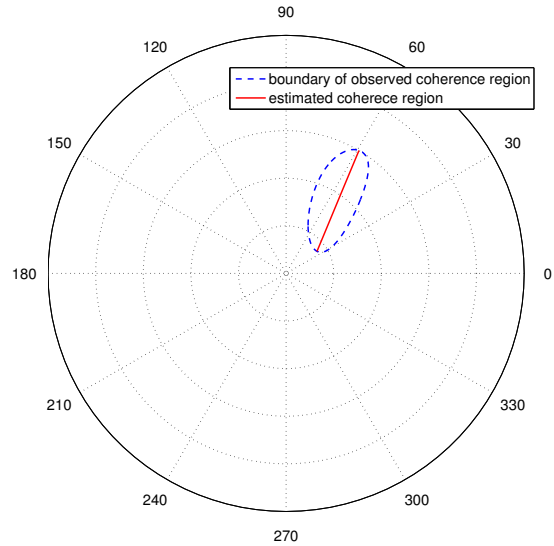


Fig. 7. Coherence estimation result for "target B" (see Fig. 4) by the best normal matrix approximation assuming double phase center.

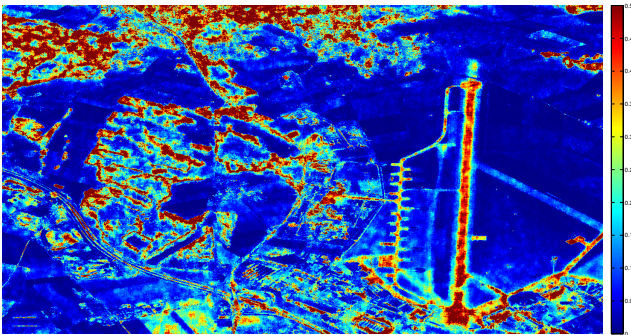


Fig. 6. Map of relative error by best normal matrix approximation assuming single phase center.

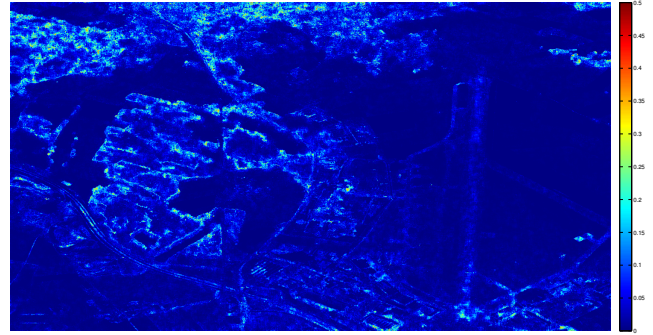


Fig. 8. Map of relative error by the best normal matrix approximation assuming double phase center.

As expected, the relative error has been indeed decreased due to the increased model order. However, one can also see that the usage of the triple phase center scattering model has not been insufficient. The relative errors of those pixels whose relative errors are large in Fig. 8 remain considerably large in Fig. 9, especially in the forest areas at the upper left of the scene. One explanation for such phenomenon is that these regions may contain more than three phase centers; or it is also possible that they contain three phase centers but the normality (and hence IPS) are unlikely to hold. Therefore both invalidate the normal matrix approximation solution. Another probable reason is that these regions suffer strong decorrelation, a fact supported by the very low coherence level in Fig. 10, where the maximum coherence map based on coherence optimization [12] is displayed. Such low coherence could be possibly caused by a sudden wind disturbance [34] and so complicates the scattering model discussed so far. How the

wind-induced temporal decorrelation affects the RoVG model is analyzed in [34] but its quantitative effect on the normal matrix approximation solution requires further investigation.

IX. CONCLUSION

We have theoretically demonstrated that the whitened interferometric cross-correlation matrix is normal for generic scattering models containing up to three phase centers. Such property naturally motivates a unified and efficient approach, i.e., the best normal matrix approximation solution for coherence estimation. Using both simulated and real data, we have demonstrated that the proposed solution compares favorably with several existing methods, which proves itself a promising alternative for PolInSAR application.

In addition, we emphasize the limit of the proposed method. It does not function when the resolution cell contains more than three phase centers. We have also shown that even if there

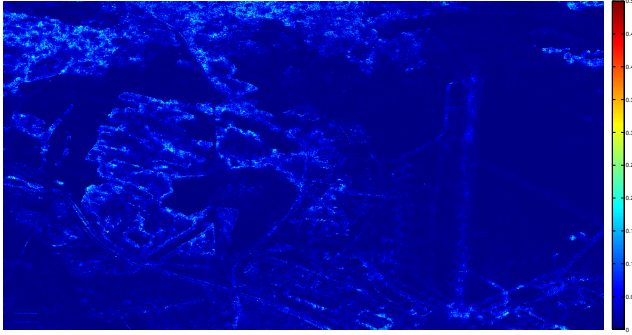


Fig. 9. Map of relative error by best normal matrix approximation assuming triple phase center.

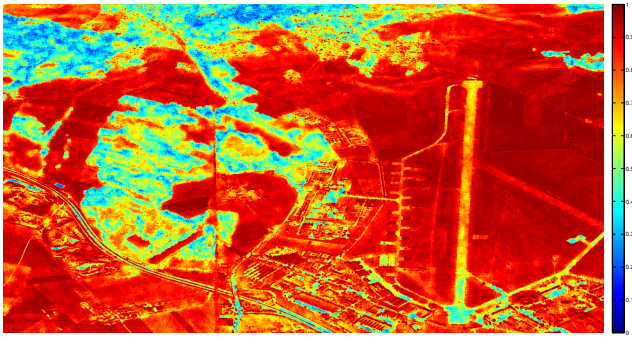


Fig. 10. Map of maximum coherence using the optimum scattering mechanism.

are only three phase centers, the normality cannot be always guaranteed. In these cases, discrimination of the scatterers cannot completely be accomplished by single-baseline PolInSAR whereas multi-baseline SAR interferometry or tomography [11] should be applied instead.

APPENDIX A

In this appendix, we derive the solution to the optimization problem (20). We first rewrite the minimizer as:

$$\Delta = \left\| (a\mathbf{B} + c\mathbf{I}_3) - \tilde{\mathbf{\Omega}}_{12} \right\|_{\text{F}}^2. \quad (56)$$

Note that $\|\mathbf{A}\|_{\text{F}}^2 = \text{Tr}(\mathbf{A}\mathbf{A}^{\text{H}})$ and $\mathbf{B} = \mathbf{B}^{\text{H}}$. Then the above equation can be further written as:

$$\Delta = \text{Tr} \left(|a|^2 \mathbf{B}^2 + ac^* \mathbf{B} - a\mathbf{B}\tilde{\mathbf{\Omega}}_{12}^{\text{H}} + ca^* \mathbf{B} + |c|^2 \mathbf{I}_3 - c\tilde{\mathbf{\Omega}}_{12}^{\text{H}} - a^* \tilde{\mathbf{\Omega}}_{12} \mathbf{B} - c^* \tilde{\mathbf{\Omega}}_{12} + \tilde{\mathbf{\Omega}}_{12} \tilde{\mathbf{\Omega}}_{12}^{\text{H}} \right). \quad (57)$$

Next we obtain the derivative of Δ with respect to \mathbf{B} . However, caution must be paid due to the additional Hermitian constraint of \mathbf{B} . Thus strictly speaking, the complex-valued matrix differentiation techniques summarized in [35] cannot be directly applied. Nevertheless, in practice, we can proceed without considering the Hermitian constraint and check whether the final solution to \mathbf{B} is indeed Hermitian. By this approach, the

derivative of Δ with respect to \mathbf{B} is given by:

$$\frac{\partial \Delta}{\partial \mathbf{B}} = 2|a|^2 \mathbf{B}^{\text{T}} + ac^* \mathbf{I}_3 - a\tilde{\mathbf{\Omega}}_{12}^* + ca^* \mathbf{I}_3 - a^* \tilde{\mathbf{\Omega}}_{12}^{\text{T}}. \quad (58)$$

Letting $\frac{\partial \Delta}{\partial \mathbf{B}} = 0$ leads to:

$$\mathbf{B} = \frac{1}{2|a|^2} \left[a\tilde{\mathbf{\Omega}}_{12}^{\text{H}} + a^* \tilde{\mathbf{\Omega}}_{12} - (ac^* + ca^*) \mathbf{I}_3 \right]. \quad (59)$$

From (59) it can be easily verified that \mathbf{B} is indeed Hermitian which confirms the validity of the above solution.

Next we substitute (59) back to (56). With some straightforward derivation it is found that Δ can be expressed in a more compact form as:

$$\Delta = \left\| \frac{1}{2z} \left(z\tilde{\mathbf{\Omega}}_{12} + z^* \tilde{\mathbf{\Omega}}_{12}^{\text{H}} + \mathbf{I}_3 \right) \right\|_{\text{F}}^2, \quad (60)$$

where

$$z = \frac{a^*}{ac^* - ca^*}. \quad (61)$$

It is clearly from (60) that minimization of Δ with respect to a and c is equivalent to minimization with respect to a single complex variable z . Suppose the polar coordinate format of z is

$$z = \rho(\cos \theta + j \sin \theta). \quad (62)$$

Also let:

$$\mathbf{H}_1 = \frac{1}{2} \left(\tilde{\mathbf{\Omega}}_{12} + \tilde{\mathbf{\Omega}}_{12}^{\text{H}} \right), \quad (63)$$

$$\mathbf{H}_2 = \frac{1}{2j} \left(\tilde{\mathbf{\Omega}}_{12} - \tilde{\mathbf{\Omega}}_{12}^{\text{H}} \right). \quad (64)$$

Considering (62)–(64) and neglecting the multiplicative constant that is irrelevant to the minima, (60) can be expanded as:

$$\Delta = \frac{D \cos \theta}{\rho} + \frac{E \sin \theta}{\rho} + \frac{F}{\rho^2} + A \cos^2 \theta + B \cos \theta \sin \theta + C \sin^2 \theta, \quad (65)$$

where

$$A = 4 \text{Tr}(\mathbf{H}_1^2), \quad (66)$$

$$B = -8 \text{Tr}(\mathbf{H}_1 \mathbf{H}_2), \quad (67)$$

$$C = 4 \text{Tr}(\mathbf{H}_2^2), \quad (68)$$

$$D = 4 \text{Tr}(\mathbf{H}_1), \quad (69)$$

$$E = -4 \text{Tr}(\mathbf{H}_2), \quad (70)$$

$$F = 3. \quad (71)$$

Minimizing (65) with respect to ρ leads to:

$$\rho = -\frac{2F}{D \cos \theta + E \sin \theta}. \quad (72)$$

Substituting the above equation back into (65) and re-arranging the sine/cosine terms we have:

$$\Delta = X \cos 2\theta + Y \sin 2\theta + Z, \quad (73)$$

where

$$X = \frac{1}{2} (4AF - D^2 - 4CF + E^2), \quad (74)$$

$$Y = 2BF - DE, \quad (75)$$

$$Z = 2AF + 2CF - \frac{1}{2}(D^2 + E^2). \quad (76)$$

Obviously, the minima of (73) is given by:

$$\theta = \frac{1}{2} [\text{atan2}(Y, X) + \pi], \quad (77)$$

Finally, according to (59) and (61), the best normal matrix approximation to $\tilde{\Omega}_{12}$ becomes:

$$\hat{\tilde{\Omega}}_{12} = \frac{1}{2z} \left(z\tilde{\Omega}_{12} - z^* \tilde{\Omega}_{12}^H - \mathbf{I}_3 \right). \quad (78)$$

The aforementioned procedure has been summarized in Algorithm 1 in Section IV.

APPENDIX B

In this appendix, we derive the condition that should be satisfied by \mathbf{T}_i in (21) and (22) in order for $\tilde{\tilde{\Omega}}_{12}$ to be normal. We first prove the following lemma.

Lemma 1. Let $\Delta_{i,j} = \mathbf{T}_i \bar{\mathbf{T}}^{-1} \mathbf{T}_j - \mathbf{T}_j \bar{\mathbf{T}}^{-1} \mathbf{T}_i$ where $\bar{\mathbf{T}} = \sum_{k=1}^3 \mathbf{T}_k$. Then $\Delta_{1,2} = \Delta_{2,3} = \Delta_{3,1}$.

Proof. As defined, we have

$$\begin{aligned} \Delta_{1,2} &= \mathbf{T}_1 \bar{\mathbf{T}}^{-1} \mathbf{T}_2 - \mathbf{T}_2 \bar{\mathbf{T}}^{-1} \mathbf{T}_1 \\ &= (\bar{\mathbf{T}} - \mathbf{T}_2 - \mathbf{T}_3) \bar{\mathbf{T}}^{-1} \mathbf{T}_2 - \mathbf{T}_2 \bar{\mathbf{T}}^{-1} (\bar{\mathbf{T}} - \mathbf{T}_2 - \mathbf{T}_3) \\ &= \mathbf{T}_2 \bar{\mathbf{T}}^{-1} \mathbf{T}_3 - \mathbf{T}_3 \bar{\mathbf{T}}^{-1} \mathbf{T}_2 \\ &= \Delta_{2,3}. \end{aligned} \quad (79)$$

Similarly, $\Delta_{2,3} = \Delta_{3,1}$. \square

Next, notice that the normality of $\tilde{\tilde{\Omega}}_{12} = \bar{\mathbf{T}}^{-\frac{1}{2}} \tilde{\Omega}_{12} \bar{\mathbf{T}}^{-\frac{1}{2}}$ requires:

$$\tilde{\tilde{\Omega}}_{12} \tilde{\tilde{\Omega}}_{12}^H - \tilde{\tilde{\Omega}}_{12}^H \tilde{\tilde{\Omega}}_{12} = \mathbf{0}, \quad (80)$$

which is equivalent to

$$\tilde{\tilde{\Omega}}_{12} \bar{\mathbf{T}}^{-1} \tilde{\Omega}_{12}^H - \tilde{\tilde{\Omega}}_{12}^H \bar{\mathbf{T}}^{-1} \tilde{\Omega}_{12} = \mathbf{0}. \quad (81)$$

Now we replace $\tilde{\tilde{\Omega}}_{12}$ with (22) for the above equation. After some necessary re-arrangement, (81) becomes:

$$\Im(\gamma_1 \gamma_2^*) \Delta_{1,2} + \Im(\gamma_2 \gamma_3^*) \Delta_{2,3} + \Im(\gamma_3 \gamma_1^*) \Delta_{3,1} = \mathbf{0}. \quad (82)$$

Therefore, according to Lemma 1, the above equation holds for all $\gamma_i \in \mathbb{C}$ iff $\Delta_{i,j} = \mathbf{0}$.

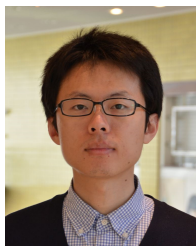
ACKNOWLEDGMENT

The authors would like to thank Dr. Kostas Papathanassiou for providing the E-SAR polarimetric interferometric data. The authors would also like to thank Dr. Jong-Sen Lee for carefully reading the manuscript and his suggestions to improve the presentation. Last but not least, the authors acknowledge the anonymous reviewers and editors for their constructive comments to make this paper better.

REFERENCES

- [1] J.-S. Lee and E. Pottier, *Polarimetric Radar Imaging: From Basics to Applications*, CRC Press, 2009.
- [2] S. Cloude, *Polarisation: Applications in Remote Sensing*, Oxford University Press, 2010.
- [3] J. van Zyl and Y.-J. Kim, *Synthetic Aperture Radar Polarimetry*, John Wiley & Sons, 2011.
- [4] C. Lopez-Martinez and X. Fabregas, "Polarimetric SAR speckle noise model," *IEEE Trans. Geosci. Remote Sens.*, vol. 41, no. 10, Oct. 2003.
- [5] I. Hajnsek, E. Pottier, and S. Cloude, "Inversion of surface parameters from polarimetric SAR," *IEEE Trans. Geosci. Remote Sens.*, vol. 41, no. 4, pp. 727-774, pp. 2232-2242, Apr. 2003.
- [6] J. Yang, Y. Peng, and S. Lin, "Similarity between two scattering matrices," *Electronics Letters*, vol. 37, no. 3, pp. 193-194, Feb. 2001.
- [7] J. Yang, G. Dong, Y. Peng, Y. Yamaguchi, and H. Yamada, "Generalized optimization of polarimetric contrast enhancement," *IEEE Geosci. Remote Sens. Letters*, vol. 1, no. 3, pp. 171-174, Jul. 2004.
- [8] S. Cloude and E. Pottier, "An entropy based classification scheme for land applications of polarimetric SAR," *IEEE Trans. Geosci. Remote Sens.*, vol. 35, no. 1, pp. 68-78, Jan. 1997.
- [9] A. Freeman and S. Durden, "A three-component scattering model for polarimetric SAR data," *IEEE Trans. Geosci. Remote Sens.*, vol. 36, no. 3, pp. 963-973, Jan. 1997.
- [10] R. Bamler and P. Hartl, "Synthetic aperture radar interferometry," *Inverse Problems*, vol. 14, no. 4, pp. R1-R54, 1998.
- [11] A. Reigber and A. Moreira, "First demonstration of airborne SAR tomography using multibaseline L-band data," *IEEE Trans. Geosci. Remote Sens.*, vol. 38, no. 5, pp. 2142-2152, Sep. 2000.
- [12] S. Cloude and K. Papathanassiou, "Polarimetric SAR interferometry," *IEEE Trans. Geosci. Remote Sens.*, vol. 36, no. 5, pp. 1551-1565, Sep. 1998.
- [13] K. Papathanassiou and S. Cloude, "Single-baseline polarimetric SAR interferometry," *IEEE Trans. Geosci. Remote Sens.*, vol. 39, no. 11, pp. 2352-2363, Nov. 2001.
- [14] T. Flynn, M. Tabb, and R. Carande, "Coherence region shape extraction for vegetation parameter estimation in polarimetric SAR interferometry," in *Proc. IGARSS*, Toronto, Canada, June 2002, vol. 5, pp. 2596-2598.
- [15] M. Tabb, J. Orrey, T. Flynn, and R. Carande, "Phase diversity: a decomposition for vegetation parameter estimation using polarimetric SAR interferometry," in *Proc. EUSAR*, Cologne, Germany, June 2002, pp. 721-724.
- [16] E. Colin, C. Titin-Schnaider, and W. Tabbara, "An interferometric coherence optimization method in radar polarimetry for high-resolution imagery," *IEEE Trans. Geosci. Remote Sens.*, vol. 44, no. 1, pp. 167-175, Jan. 2006.
- [17] R. Treuhhaft and P. Siqueira, "The vertical structure of vegetated land surfaces from interferometric and polarimetric radar," *Radio Sci.*, vol. 35, no. 1, pp. 141-177, 2000.
- [18] S. Cloude and K. Papathanassiou, "Three-stage inversion process for polarimetric SAR interferometry," *IEE Proc. Radar Sonar Navig.*, vol. 150, no. 3, pp. 125-134, June. 2003.
- [19] L. Ferro-Famil, M. Neumann, and Y. Huang, "Multi-baseline POL-InSAR statistical techniques for the characterization of distributed media," *Proc. IGARSS*, vol. 3, pp. III971-III974, 2009.
- [20] C. Lopez-Martinez and A. Alonso-Gonzalez, "Assessment and estimation of the RVoG model in polarimetric SAR interferometry," *IEEE Trans. Geosci. Remote Sens.*, in press.
- [21] H. Yamada, Y. Yamaguchi, Y.-J. Kim, E. Rodriguez, and W.M. Boerner, "Polarimetric SAR interferometric for forest analysis based on the ESPRIT algorithm," *IEICE Trans. Electron.*, vol. E84-C, pp. 1917-1924, Dec. 2001.
- [22] S. Guillaso, A. Reigber, and L. Ferro-Famil, "Evaluation of the ESPRIT approach in polarimetric interferometric SAR," in *Proc. IGARSS*, vol. 1, 2005.
- [23] S. Guillaso, L. Ferro-Famil, A. Reigber, and E. Pottier, "Building characterization using L-band polarimetric interferometric SAR data," *IEEE Geosci. Remote Sens. Letter*, vol. 2, no. 3, pp. 347-351, 2005.
- [24] S.-W. Chen, X. Wang, and M. Sato, "PolInSAR Complex Coherence Estimation Based on Covariance Matrix Similarity Test," *IEEE Trans. Geosci. Remote Sens.*, vol. 50, no. 11, pp. 4699-4710, Nov. 2012.
- [25] F. Zachlin, Paul, and Michiel E. Hochstenbach, "On the numerical range of a matrix: By Rudolf Kippenhahn (1951 in Bomberg)," *Linear and Multilinear Algebra*, vol. 56, no. 1-2, pp. 185-225, 2008.
- [26] D.S. Keeler, L. Rodman, and I.M. Spitkovsky, "The numerical range of 3 3 matrices. Linear algebra and its applications," vol. 252, no. 1, pp. 115-139, 1997.

- [27] M. Neumann, *Remote sensing of vegetation using multi-baseline polarimetric SAR interferometry: theoretical modeling and physical parameter retrieval*, Ph.D. thesis, Université de Rennes 1, France, Jan. 2009.
- [28] I. Hajnsek, F. Kugler, S.-K. Lee, and K.P. Papathanassiou, "Tropical-forest-parameter estimation by means of Pol-InSAR: The INDREX-II Campaign," *IEEE Trans. Geosci. Remote Sens.*, vol. 47, no. 2, pp. 481-493, Feb. 2009.
- [29] K. Gustafson and D. Rao, *The Field of Values of Linear Operators and Matrices*, Springer-Verlag, 1997.
- [30] M. Neumann, A. Reigber, and L. Ferro-Famil, "POLInSAR Coherence Set Theory and Application," in *Proc. EUSAR*, Dresden, Germany, May 2006.
- [31] A. Ruhe "Closest normal matrix finally found!," *BIT Numerical Mathematics*, vol. 27, no. 4, pp. 585-598, 1987.
- [32] [Online]: http://perso.telecom-paristech.fr/~cardoso/Algo/Joint_Diag/joint_diag.m
- [33] J.-S. Lee, T.L. Ainsworth, and K.-S. Chen, "Speckle Filtering of Dual-Polarization and Polarimetric SAR Data based on Improved Sigma Filter," *Proc. IGARSS*, vol. 4, pp. IV21-IV24, 2008.
- [34] S.-K. Lee, F. Kugler, K.P. Papathanassiou, and I. Hajnsek, "Quantification of temporal decorrelation effects at L-band for polarimetric SAR interferometry applications," *IEEE J. Select. Topics Appl. Earth Observ. Remote Sens.*, vol. 6, pp. 1351-1367, June 2013.
- [35] A. Hjørungnes and D. Gesbert, "Complex-Valued Matrix Differentiation: Techniques and Key Results," *IEEE Trans. Signal Process.*, vol. 55, no. 6, pp. 2740-2746, June. 2007.



Yi Cui (S'09-M'11) received the B.S. degree (with honors) in electronic information science and technology from the College of Electronic Science and Engineering of Jilin University, Changchun, China, in 2006. From 2006 to 2011 he was a doctoral student at Tsinghua University, Beijing, China and received the Ph.D. degree in information and communication engineering from the Department of Electronic Engineering of Tsinghua University in 2011. From 2011 to 2013, he was a post-doctoral fellow at Niigata University where he is now an

assistant professor.

Dr. Cui was the first-prize winner of the student paper competition at the 2010 Asia-Pacific Radio Science Conference (AP-RASC10), the recipient of the Best Paper Award of the 2012 International Symposium on Antennas and Propagation (ISAP), and the recipient of 2013 IEEE GRSS Symposium Prize Paper Award. He has been recognized as the 2013 Best Reviewer of IEEE TRANSACTIONS ON GEOSCIENCE AND REMOTE SENSING. He is an associate editor of IEEE JOURNAL OF SELECTED TOPICS IN APPLIED EARTH OBSERVATION AND REMOTE SENSING.



Yoshio Yamaguchi (M'83-SM'94-F'02) received the B.E. degree in electronics engineering from Niigata University, Niigata, Japan, in 1976 and the M.E. and Dr. Eng. degrees from Tokyo Institute of Technology, Tokyo, Japan, in 1978 and 1983, respectively.

In 1978, he joined the Faculty of Engineering, Niigata University. From 1988 to 1989, he was a Research Associate at the University of Illinois at Chicago, Chicago. His interests are in the field of radar polarimetry, microwave sensing, and imaging.

Dr. Yamaguchi has served as Chair of IEEE Geoscience & Remote Sensing Society (GRSS) Japan Chapter (2002-2003), Chair of International Union of Radio Science Commission F Japanese Committee (URSI-F) Japan (2006-2011), Associate Editor for Asian affairs of GRSS Newsletter (2003-2007), and Technical Program Committee (TPC) Co-Chair of the 2011 IEEE International Geoscience and Remote Sensing Symposium (IGARSS). He is a Fellow of the Institute of Electronics, Information and Communication Engineers (IEICE), Japan, and a recipient of the 2008 IEEE GRSS Education Award.



Hiroyoshi Yamada (M'93) received the B.E., M.E., and Dr. Eng. degrees in electronic engineering from Hokkaido University, Sapporo, Japan, in 1988, 1990, and 1993, respectively.

Since 1993, he has been with the Faculty of Engineering, Niigata University, Niigata, Japan, where he is currently a Professor. From 2000 to 2001, he was a Visiting Scientist at the Jet Propulsion Laboratory, California Institute of Technology, Pasadena. His research interests include array signal processing, polarimetric radar interferometry, radar, and high-

resolution DOA estimation techniques.

Dr. Yamada is the Chair of the IEEE Antennas and Propagation Society, Japan Chapter (2013- current). He is a senior member of The Institute of Electronics, Information and Communication Engineers (IEICE) of Japan, and is an Editor-in-Chief of the IEICE Communications Express, and was the recipient of the 2010 Best Paper Award of IEICE.



Sang-Eun Park (S'05-M'07) received the B.S. and M.S. degrees in geophysics and Ph.D. degree in radar remote sensing and geophysics from the Seoul National University, Seoul, Korea, in 2000, 2002, and 2007 respectively. From 2007 to September 2009, he worked at the Radar Polarimetry Remote Sensing Group of the University of Rennes 1, Rennes, France, for a post-doctoral fellow on radar polarimetry. From October 2009 to January 2010, he was a project scientist in the Institute of Photogrammetry and Remote Sensing, Vienna

University of Technology, Vienna, Austria. From February 2010 to February 2014, he was an Assistant Professor in the Graduate School of Science and Technology at Niigata University, Japan. He is currently an Assistant Professor in the Geoinformation Engineering at Sejong University, Korea. His research interests include polarimetric SAR classification, forward and inverse modeling of microwave vegetation and surface backscattering, and investigation of multi-source data integration methodology